

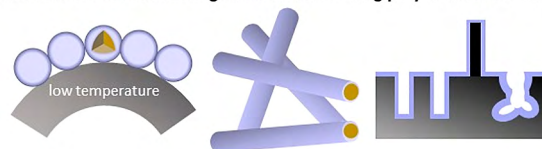
Three-Dimensional (3D) Device Architectures Enabled by Oxidative Chemical Vapor Deposition (oCVD)

Karen K. Gleason* 

^a Department of Chemical Engineering, Massachusetts Institute of Technology, Cambridge, MA 02139, USA

* kkg@mit.edu

oxidative CVD of conducting and semiconducting polymers for 3D devices




• conformality • electrical, ionic, & optical conductivity • flexibility •

Received: 19.07.2022

Accepted after revision: 02.09.2022

DOI: 10.1055/a-1982-7432; Art ID: OM-2022-07-0024-SR

License terms: 

© 2022. The Author(s). This is an open access article published by Thieme under the terms of the Creative Commons Attribution-NonDerivative-NonCommercial License, permitting copying and reproduction so long as the original work is given appropriate credit. Contents may not be used for commercial purposes, or adapted, remixed, transformed or built upon. (<https://creativecommons.org/licenses/by-nc-nd/4.0/>)

Abstract For fabricating devices with three-dimensional (3D) architectures, oxidative chemical vapor deposition (oCVD) offers conformal nano-coatings of polymers with designable composition. Pure, uniform, and pinhole-free oCVD layers are achievable with sub-10 nm thickness and sub-1 nm roughness. The low substrate temperature used for oCVD allows direct deposition on to the thermally sensitive substrates desired for flexible and wearable devices. The oCVD polymers can graft to the underlying material. The covalent chemical bonds to the substrate create a robust interface that prevents delamination during the subsequent device fabrication steps and exposure to the environmental conditions of device operation. Both electrically conducting and semiconducting polymers have been synthesized by oCVD. Small ions act as dopants. The oCVD process allows for systematic tuning of electrical, optical, thermal, and ionic transport properties. Copolymerization with oCVD can incorporate specific organic functional groups into the resulting conjugated organic materials. This short review highlights recent examples of using oCVD polymer to fabricate organic and hybrid organic-inorganic devices. These optoelectronic, electrochemical, and sensing devices utilize 3D architectures made possible by the conformal nature of the oCVD polymers.

Introduction

oCVD Chemistry and Process

Optoelectronic Devices

Electrochemical Devices

Sensing Devices

Conclusions and Outlook

Key words: oxidative chemical vapor deposition (oCVD), polyethylenedioxythiophene (PEDOT), optoelectronic devices, electrochemical devices, sensors, polymers

Introduction

Chemical vapor deposition (CVD) has been widely adopted by the semiconductor industry to grow thin films of inorganic materials.¹ High-purity films and interfaces are made possible by the ease of purifying the small volatile molecules used as reactants for CVD, the use of vacuum processing, and in vacuo transfer between process steps. Additionally, CVD allows in the film thickness to be controlled with nanometer precision in real time during growth and can achieve uniformity in composition and thickness across the silicon wafer.

The purity, thickness control, and uniformity of CVD processing extends to the growth of organic polymer films.^{2,3} Additionally, CVD polymers can form covalent chemical bonds to the substrate. This grafting creates robust interfaces that resist delamination. Hence, grafted oCVD polymers can survive subsequent device process steps and the environmental conditions of device operation. The substrate temperatures used for oCVD are typically between ~25 °C and ~140 °C. These low substrate temperatures permit oCVD polymers to grow directly on top of thermally sensitive materials. Most ordinary materials, such as papers, plastics, and textiles, have limited thermal stability. These ubiquitous substrates are essential for fabricating flexible and wearable devices. Thus, the low growth temperature of oCVD provides a distinct advantage over processes requiring higher substrate temperatures, such as those for CVD graphene. When the process temperature is higher than the substrate can withstand, costly and complex transfer steps from a sacrificial substrate are needed. In contrast, oCVD is a single-step process for fabrication directly on thermally sensitive materials.

Multiple methods of CVD polymerization have been developed, each producing a specific subclass of polymers.³ The oxidative CVD (oCVD) technique is utilized for conjugated polymers. The oCVD electrically conducting and semiconducting films can be ultrathin (< 10 nm), ultrasmooth (root mean square roughness < 1 nm), and grown conformally over nanostructured surfaces. The current review focuses on recent advances in utilizing oCVD for fabricating

Biosketch



Karen K. Gleason is the Alexander and I. Michael Kasser Professor of Chemical Engineering, Emerita at MIT. She is a member of the U.S. National Academy of Engineering and a Fellow of the American Institute of Chemical Engineering (AIChE). Dr. Gleason's honors from the AIChE include the 2021 Margaret Hutchinson Rousseau Pioneer Award for Lifetime Achievement by a Women Chemical Engineer, the 2019 Institute Lecturer Award, and 2015 Charles Stine Award. Her publications include > 350 journal articles, 3 books, and > 40 U.S. patents. More than 20 of Prof. Gleason's research advisees hold tenured or tenure-track faculty positions. Ten of these happen to be women. Dr. Gleason served in a series of leadership positions at MIT, including Associate Provost, Associate Dean of Engineering, Associate Director for the Institute of Soldier Nanotechnologies, and Executive Officer of the Chemical Engineering Department. Her Ph.D. was awarded from the University of California at Berkeley, and her B.S. and M.S. degrees are from MIT, where she also won All-American honors in swimming.

novel optoelectronic, electrochemical, and sensing devices having three-dimensional (3D) architectures.

oCVD Chemistry and Process

In oCVD, polymers with conjugated backbones are formed by the step-growth mechanism.² Numerous oCVD homopolymers and copolymers have been demonstrated. Figure 1 shows thiophene and related oCVD monomers, including 3-methylthiophene (3MT), 3-hexylthiophene, 3,4-dimethoxythiophene, 3-thiophene acetic acid (TAA), 3-thiophene ethanol, 3,4-ethylenedioxythiophene (EDOT), 3,4-propylenedioxythiophene (ProDOT), and 3,4-ethylenediathia thiophene (EDTT). Additionally, oCVD monomers include, but are not limited to, aniline, pyrrole, selenophene and their derivatives, as well as 1,3-dihydroisothianaphthene (DHITN), dopamine, and metal porphyrins.

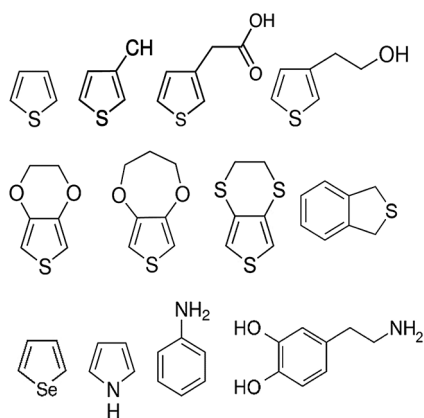


Figure 1 Chemical structures for selected oCVD monomers. From left to right, (top row) thiophene, 3MT, TAA, TE; (2nd row) EDOT, ProDOT, EDTT, DHITN; (3rd row) selenophene, pyrrole, aniline, and dopamine.

The oxidant can be supplied by sublimation of a solid, such as FeCl_3 , CuCl_2 , or MoCl_5 ; vaporization of a liquid, such as VOCl_3 , SbCl_5 , or H_2SO_4 ; or directly as a gas, such as Br_2 .² On the growth surface inside the oCVD reaction chamber, the monomer and oxidant adsorb and spontaneously react. No light source, plasma generator, or heated filaments are required. The oxidant both polymerizes the monomer and produces the doping of the oCVD polymer. Controlling the oxidant concentration at the surface is key for retaining the integrity of the substrates, enabling the successful device fabrication described in this review.

The introduction of the volatile liquid oxidants VOCl_3 and SbCl_5 by Lau was a major advance for oCVD.^{4,5} The VOCl_3 and SbCl_5 oxidants tend to produce volatile reaction byproducts which release gas as the oCVD film grows, eliminating the need for a post-deposition rinsing step. The vapors from the volatile liquid oxidants can be introduced by a feed system similar to the one used for monomer. Introducing the oxidant as a vapor improves the ability to control the partial pressure of the oxidant in the chamber and to achieve the desired stoichiometry relative to the monomer feed. The external oxidant vapor feed system also allows more flexibility in the geometric design of the vacuum reaction chamber (Figure 2).

With the SbCl_5 oxidant, uniform oCVD PEDOT was reported over 10-cm diameter silicon wafers.⁶ In some cases, additional vapor-phase reactants, such as water or pyridine; or carrier gases, such as N_2 , are utilized along with the monomers and oxidants. Alternating periods of monomer-only and oxidant-only flow is termed oxidative molecular layer deposition (oMLD). The oMLD growth rates are 100-fold slower than oCVD and the resulting oMLD film properties have not yet matched those of oCVD.⁷

When carbon-carbon double bonds are present at the surface of the substrate, the oxidant can induce grafting of the oCVD polymer.² The covalent chemical bonds which span across the interface improve durability. Robust interfaces help prevent delamination of the oCVD layers. Delamination during a multi-step fabrication process leads to the failure to produce devices. Delamination can also result due to

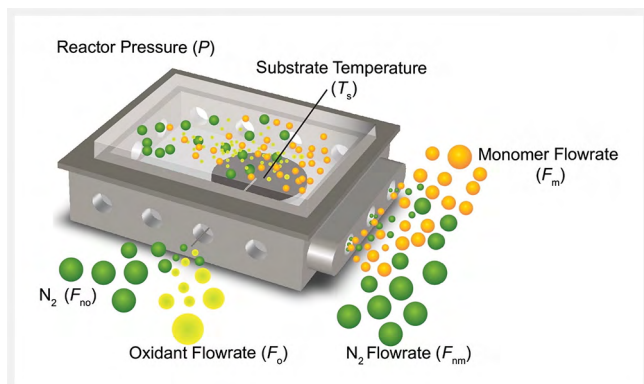


Figure 2 Schematic of an oCVD chamber utilizing a monomer, a volatile oxidant, and a N_2 carrier gas for the growth of oCVD-conjugated polymers. Reprinted with permission from Ref. 5. Copyright 2018 Elsevier.

the temperature, humidity, salt exposure, mechanical flexing, and other environmental conditions experienced by the device during use and lead to complete device failure. Chemical modification of the surface can also be used to control the orientation of the grafted oCVD polymer chain. The influence of surface chemistry was used to achieve self-aligned patterns of oCVD PEDOT over lines of silicon dioxide.⁷ Between the lines, inhibition of oCVD growth occurred, as the hydrogen-terminated silicon surface reduced the absorbing oxidants.

Optoelectronic Devices

Several oCVD polymers have high electrical conductivity, σ . The highest σ value reported is for oCVD PEDOT, $7520 \pm 240 \text{ S}\cdot\text{cm}^{-1}$, which was achieved using water-assisted growth with the volatile $SbCl_5$ oxidant to deposit face-on-oriented thin films.⁸ Electrical conductivity combined with optical transparency makes oCVD PEDOT attractive as a flexible transparent electrode.⁹ The oxidant and oCVD process conditions strongly influence the optoelectronic properties achieved.⁹ More research is required to understand the observed trends.

The $SbCl_5$ oxidant also resulted in the highest σ values for oCVD polythiophene⁴ and polypyrrole¹⁰ of 70 and 180 $\text{S}\cdot\text{cm}^{-1}$, respectively. For oCVD poly-(3,4-ethylenedithia thiophene) (PEDTT), the all-sulfur analog of PEDOT, σ values $> 1000 \text{ S}\cdot\text{cm}^{-1}$ were achieved using H_2SO_4 as the volatile oxidant.¹¹

Hybrid organic-inorganic light-emitting diodes (LEDs) were fabricated using hole-conductive oCVD PEDOT as the p-type contact for gallium nitride (GaN).¹² The hybrid interface oCVD PEDOT with GaN was successfully modelled as an ideal Schottky barrier, confirming the quasi-metallic state of the oCVD PEDOT with a work function of approximately

-5.3 eV . Both current spreading and hole injection were improved when oCVD PEDOT was substituted in place of p-GaN. Hybrid planar LEDs exhibited excellent thermal and temporal stability and achieved high rectification ratios ($> 10^7$ at $\pm 2 \text{ V}$). Enhanced current spreading during electroluminescence measurements was achieved using oCVD PEDOT as a pinhole-free conformal p-type contact over 3D microrods. The microrod structure consisted of an n-type GaN core, covered in an InGaN multi-quantum well structure, and capped with a p-type AlGaN blocking layer. Figure 3 shows the conformal coverage by $\sim 60 \text{ nm}$ thick oCVD PEDOT, while bridging defects between microrods resulted when PEDOT:PSS was spin-coated. The demonstration of the oCVD PEDOT-encapsulated microrods is an important step towards achieving 3D LEDs with high aspect ratios. As compared to planar LEDs, 3D architectures provide higher surfaces for light emission and have the potential to reduce both fabrication costs and defect incorporation.

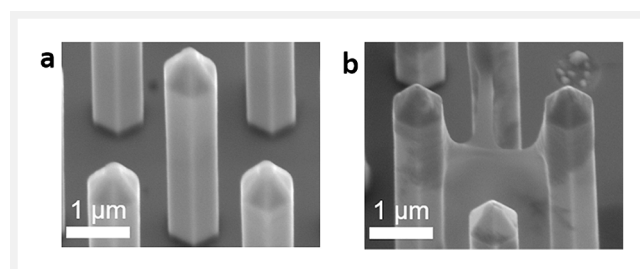


Figure 3 Scanning electron micrographs (SEMs) of GaN microrod structures (a) conformally coated with 60 nm thick oCVD PEDOT, and (b) non-conformally coated with spin-coated PEDOT:PSS. The surface tension during solution application of PEDOT:PSS results in a bridging defect that spans in between multiple microrods. Adapted from Ref. 12 published under a creative commons license (CC BY).

Hybrid nanostructured photodetectors have been demonstrated using oCVD PEDOT.¹³ Photodetectors are essential for a wide range of applications including night vision, motion tracking, and bio-sensing. Photons are readily captured by a nanostructured form of silicon known as black silicon (b-Si). However, defects at the surfaces of b-Si often lead to undesired recombination of the photo-induced electron-hole pairs. These recombination events reduce the efficiency of charge extraction. Conformal growth of oCVD PEDOT over b-Si both passivates the surface defects and provides high electrical conductivity ($3000 \text{ S}\cdot\text{cm}^{-1}$) pathways to facilitate charge extraction. Charge extraction at the heterogeneous interface was further enhanced by the forming covalent chemical bonds between b-Si and the EDOT monomer at the start of the oCVD process. The oCVD PEDOT conformally covered the porous architecture of the b-Si, having pore diameters ranging from 40 to 500 nm and pore depths of less than 500 nm. In contrast, spin-coated PEDOT:PSS did not conformally cover the b-Si, leaving many surfaces unpassi-

vated and forming bridging defects encompassing multiple nanostructures, similar to the observation for 3D microrod structures (Figure 3b). An unprecedented finding was that by changing only the bias applied during detection, a single hybrid oCVD PEDOT/b-Si photodetector could separately extract near-IR and visible light information. This dual functionality was achieved without requiring a filter.

Organic and hybrid photovoltaics have utilized oCVD polymers in multiple ways.^{14,15} As hole-transport layers (HTLs), oCVD PEDOT layers between 2 and 45 nm thick have been integrated with lead sulfide quantum dots, perovskites, and organic semiconductors. As an HTL for dye-sensitized solar cells, oMLD PEDOT was conformally grown over mesoporous indium tin oxide (ITO). Similarly, oCVD poly(3,4-dimethylthiophene) has been demonstrated as an HTL for organic photovoltaics. Additionally, oCVD PEDOT layers between 50 and 60 nm thick formed the transparent anode in organic photovoltaic devices, including flexible and foldable solar cells on unmodified paper substrates. The oCVD organic semiconductors polyselenophene and polythiophene layers between 15 and 70 nm thick have been integrated into photovoltaic cells.

Electrochemical Devices

The use of 3D device architectures can greatly increase the surface area available for electrochemical processes.¹⁶ However, forming complete device layers over all the internal surfaces present in geometric complex substrates is challenging. Neither line-of-sight vacuum deposition processes nor solution-based coating processes achieve the necessary coverage. However, oCVD can produce conformal coatings which provide both the electrical and ionic conductivity desired for 3D energy storage devices.^{14,17} The orientation of the crystalline domains within the oCVD layers can influence both electronic and ionic transport.

Supercapacitors have been fabricated using oCVD polymers to conformally modify a variety of nanostructured substrates.^{14,17} The resulting composite electrodes are often mechanically flexible, as desired for wearable devices and for ready shaping for integration into vehicle parts. The small ionic dopants in the oCVD polymers provide an intrinsic mechanism for pseudocapacitive charge storage. The maximum specific pseudocapacitance corresponds to the uptake of one dopant counter ion per monomer unit. Due to its small monomer volume, polyaniline (PANI) has one of the highest theoretical capacities, 750 F/g, for a conducting polymer. Additional criteria, such as electrical conductivity or the electrochemical operating window, have also led to the use of other oCVD monomers including thiophene, 3MT, and EDOT.

Supercapacitors were fabricated by the conformal coating of electrospun carbon nanofiber mats with porous oCVD

PANI (Figure 4).¹⁸ The pores, ~40 nm in diameter, facilitated ionic transport. The resulting composite electrode had a specific capacitance of 149 F/g. The devices displayed high rate capability (98% capacitance retention at 600 mV/s) and excellent cycling capability (92% retention after 3000 cycles). For nonporous oCVD PANI, uniform penetration into the full depth of the mat was achieved at high oCVD substrate temperatures, where the rate-limiting step is the adsorption of reactive vapors to the substrate.¹⁹

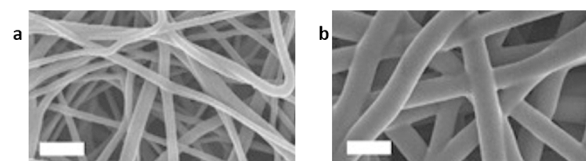


Figure 4 SEMs of carbon nanofiber mats (a) uncoated and (b) conformally modified with oCVD PANI, without webbing or bridging defects in the polymeric coating. Adapted with permission from Ref. 19. Copyright 2020 American Chemical Society.

Conformal coverage of free-standing silicon carbon nanowires by oCVD PEDOT provided an areal capacitance of 0.026 F/cm² at 0.2 mA/cm², a factor of 3.7× over the unmodified nanowires.²⁰ The device retained nearly full capacity after 10,000 cycling events.

Increased surface area and ordering of the nanostructured electrode improved energy storage performance.²¹ Densified horizontally aligned carbon nanotube (HACNT) arrays were conformally modified with oCVD poly(3-methylthiophene) (P3MT; Figure 5). The resulting area capaci-

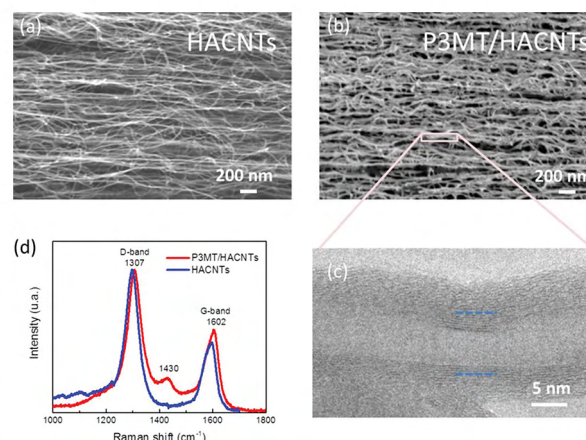


Figure 5 SEMs of HACNT arrays (a) uncoated and (b) conformally coated with an ~5 nm thick oCVD P3MT layer. (c) A transmission electron micrograph with dashed lines to indicate the HACNT/P3MT interface. (d) Raman spectra comparing the HACNT with and without the oCVD P3MT coating. Reprinted with permission from Ref. 21. Copyright 2019 John Wiley and Sons.

tance was 3.1 F/cm^2 at 5 mA/cm^2 , a factor $\sim 3\times$ higher than the unmodified nanotube array. The energy density ($1.08 \text{ mWh}\cdot\text{cm}^{-2}$) and power density ($1.75 \text{ W}\cdot\text{cm}^{-2}$) exceeded all previously reported values. Good performance was retained after 5,000 cycles and repeated, severe mechanical deformation.

Supercapacitors fabricated from oCVD PEDOT have also been integrated directly into garments.²² For wearable devices, the energy density is particularly important. The maximum energy density ($< 0.05 \text{ mWh/cm}^2$) on the garment-based device was achieved at power density ($< 0.001 \text{ W/cm}^2$), values which are respectively $> 20\times$ and $> 1000\times$ lower than reported for the flexible HACNT supercapacitors described above. The difference can be attributed in part to the lower interfacial area for pseudocapacitive charge storage when using garment substrates.

Lithium-ion batteries suffer from degradation during charging and discharging, which both shortens device lifetime and creates serious safety concerns. The oCVD PEDOT modification of cathode powders achieved enhanced stability during battery cycling.^{23–25} Conformal coverage was achieved over both the exterior surfaces and the interior surfaces of microvoids in the powders. In addition to conducting lithium ions and electrons, the oCVD PEDOT skin suppressed undesired phase transitions and mitigated mechanical cracking during the expansion and contraction experienced during electrochemical cycling.²³ Improved interfacial stability has been attributed in part to covalent bonds formed between the oCVD polymer and LiMn_2O_4 cathode powder.²⁴ Interfacial chemical bonding and the mechanical flexibility of the oCVD PEDOT greatly enhance cycling stability of Ni-rich cathodes.²⁵ With oCVD modification, 80% of capacity was retained at 300 cycles as compared to only 6% retention after 200 cycles for the unmodified powder.

Redox flow batteries are desired for long-term, large-scale stationary energy storage resulting from the variable output of sustainable sources of energy generation.²⁶ One option for stationary energy storage is redox flow batteries. Conformal oCVD PEDOT (78 nm thick) over carbon cloth electrodes was found to reduce the ohmic, kinetic, and mass transport resistances of the electrochemical reactions occurring in redox flow batteries. Galvanostatic cycling experiments demonstrated that the oCVD PEDOT provided stable electrochemical performance and remained free from delamination failures over the entire 2.9-day course of the experiment. In contrast, coating by solution-applied PEDOT:PSS gave non-conformal coverage. Bridging defects occurred between fibers treated with PEDOT:PSS, analogous to the situation for the 3D microrods (Figure 3b). Additionally, delamination failures in PEDOT:PSS coatings developed on the carbon cloth electrodes even prior to electrochemical testing. In contrast, oCVD PEDOT did not delaminate, even during testing, demonstrating the importance of a robust interface to the substrate.

Sensing Devices

Many types of sensors have been fabricated using oCVD polymers.¹⁴ Both chemoresistive sensing of volatile organic compounds and rapid biosensing utilized oCVD copolymerization to incorporate organic functional groups, such as the hydroxyl group ($-\text{OH}$) from the monomer 3-thiopheneetha-

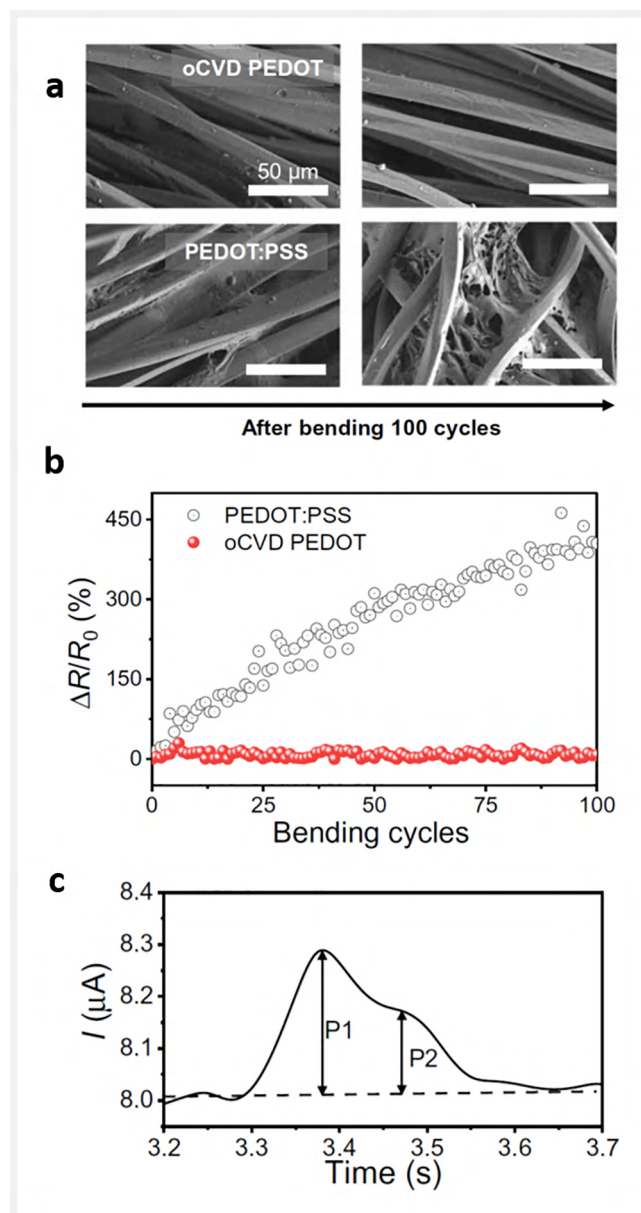


Figure 6 SEMs of polyester fabric coated with oCVD PEDOT or PEDOT:PSS before and after 100 cycles of bending and the corresponding resistance changes. The blood pressure at the wrist was recorded during a single heartbeat using a sensor fabricated by depositing and patterning of oCVD PEDOT on a polyester fabric in a single step. Reprinted from Ref. 27 published under a creative commons license (CC BY-NC).

nol and the carboxylic acid group ($-\text{COOH}$) from the monomer TAA. The organic functional groups allow post-deposition surface modification of the oCVD copolymers with molecules or nanoparticles that enhance the sensitivity and specificity of the sensors. The mobility of small anions to dope and dedope oCVD polymers in response to applied voltage enables electrochromic sensors, with the color switching characteristic controlled by the optical band gap of the materials.

Wearable sensors make use of the uniformity, conformality, and stability of oCVD PEDOT on fabrics (Figure 6).²⁷ The breathability of the fabric was retained after oCVD coating. A blood pressure sensor was fabricated on commercial polyester fabrics and gloves. An increase in pressure deforms the oCVD-coated fabric thread producing a measurable decrease in resistance. The baseline resistance value is quickly recovered when the pressure is removed. Using shadow masking, respiratory sensors were fabricated directly in a single step on commercially available disposable facial masks.

Piezoresistive sensing was demonstrated using conformal layers of oCVD PEDOT grown around microspheres of polystyrene which had been assembled into a monolayer on top of a flexible substrate (Figure 7).²⁸ The microspheres were ~ 580 nm in diameter and the oCVD thickness was ~ 50 nm. The change in resistance was measured upon bending of the device. Gauge factors as high as 11.4 were achieved.

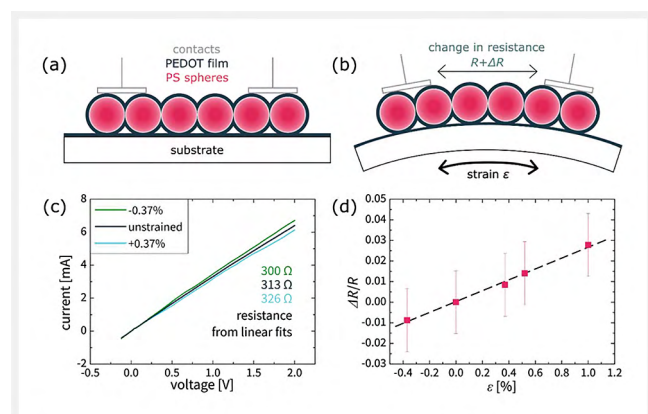


Figure 7 Schematic of piezoresistive sensors in (a) unstrained and (b) strained configurations and (c, d) the resistive response with strain. Reprinted from Ref. 28 published under a creative commons license (CC BY-NC).

Bioimpedance sensing was achieved by direct deposition of shadow-masked oCVD PEDOT-patterned electrodes on to freshly cut plant leaves.²⁹ The measured impedance at high frequency revealed damage to leaves caused by early-stage ozone exposure and drought.

Conclusions and Outlook

Polymeric nanolayers synthesized by oCVD have enabled 3D architectures for many types of devices. Low substrate temperatures allow oCVD polymers to be grown directly on top of thermally sensitive materials. The oCVD method is compatible with traditional microelectronics manufacture and also offers the conformal coverage of geometric features associated with random and ordered nanostructures. The conformal coverage results because the surface tension phenomena present in liquid-applied coatings can be avoided by vapor-phase processing. Using solvent-free methods also eliminates dewetting phenomena which form pinholes and bridging defects. Thus, oCVD results in the pinhole-free layers required for fabricating devices can be achieved on virtually any substrate, even for sub-10 nm polymer thicknesses, where dewetting poses the biggest challenge. To avoid pinhole defects, surface roughness must be low compared to the film thickness. The oCVD polymer can achieve sub-1 nm rms roughness. The lack of residual solvent and other additives used for solution processes combined with the ability to purify small-molecule reactants allows oCVD polymers to have high purity.

Both conductive and semiconductive conjugated polymers have been synthesized by oCVD. Copolymers have also been grown by oCVD. The choice of monomer and oCVD process parameters allows optimization of the electronic, optical, thermal, and mechanical properties of the resulting conjugated polymers. In a single step, the oCVD process can grow patterned layers directly on thermally sensitive substrates, including papers, plastic, and textiles. Thus, conformal oCVD polymers have enormous potential integration into next-generation 3D devices, particularly when mechanical flexibility or wearability is needed.

Conflict of Interest

The author declares no conflict of interest.

References

- (1) Spear, K. E. *Pure Appl. Chem.* **1982**, *54*, 1297.
- (2) Gleason, K. K. *Nat. Rev. Phys.* **2020**, *2*, 347.
- (3) Sun, L.; Yuan, G.; Gao, L.; Yang, J.; Chhowalla, M.; Gharahcheshmeh, M.; Gleason, K.; Choi, Y.; Hong, H.; Liu, Z. *Nat. Rev. Methods Primers* **2021**, *1*, 5.
- (4) Nejati, S.; Lau, K. K. S. *Langmuir* **2011**, *27*, 15223.
- (5) Li, X.; Rafie, A.; Smolin, Y. Y.; Simotwo, S.; Kalra, V.; Lau, K. K. S. *Chem. Eng. Sci.* **2019**, *194*, 156.
- (6) Mirabedin, M.; Vergnes, H.; Causse, N.; Vahlas, C.; Causset, B. *Appl. Surf. Sci.* **2021**, *554*, 149501.
- (7) Kim, J. S.; Parsons, G. N. *Chem. Mater.* **2021**, *33*, 9221.
- (8) Heydari Gharahcheshmeh, M.; Robinson, M. T.; Gleason, E. F.; Gleason, K. K. *Adv. Funct. Mater.* **2021**, *31*, 2008712.

- (9) Heydari Gharahcheshmeh, M.; Gleason, K. K. *Mater. Today Adv.* **2020**, *8*, 100086.
- (10) Dianatdar, A.; Miola, M.; De Luca, O.; Rudolf, P.; Picchioni, F.; Bose, R. K. *J. Mater. Chem. C* **2022**, *10*, 557.
- (11) Farka, D.; Greunz, T.; Yumusak, C.; Cobet, C.; Mardare, C. C.; Stifter, D.; Hassel, A. W.; Scharber, M. C.; Sariciftci, N. S. *Sci. Technol. Adv. Mater.* **2021**, *22*, 985.
- (12) Krieg, L.; Meierhofer, F.; Gorny, S.; Leis, S.; Splith, D.; Zhang, Z.; von Wenckstern, H.; Grundmann, M.; Wang, X.; Hartmann, J.; Margenfeld, C.; Manglano Clavero, I.; Avramescu, A.; Schimpke, T.; Scholz, D.; Lugauer, H. -J.; Strassburg, M.; Jungclaus, J.; Bornemann, S.; Spende, H.; Waag, A.; Gleason, K. K.; Voss, T. *Nat. Commun.* **2020**, *11*, 5092.
- (13) Kim, H.; Zhang, Y.; Rothschild, M.; Roh, K.; Kim, Y.; Jang, H. S.; Min, B. -C.; Lee, S. *Adv. Funct. Mater.* **2022**, *32*, 2201641.
- (14) Heydari Gharahcheshmeh, M.; Gleason, K. K. *Adv. Mater. Interfaces* **2019**, *6*, 1801564.
- (15) Heydari Gharahcheshmeh, M.; Gleason, K. K. *Energies* **2022**, *15*, 3661.
- (16) Li, W.; Bradley, L. C.; Watkins, J. J. *ACS Appl. Mater. Interfaces* **2019**, *11*, 5668.
- (17) Gleason, K. K. *J. Vac. Sci. Technol., A* **2020**, *38*, 020801.
- (18) Li, X.; Rafie, A.; Kalra, V.; Lau, K. K. *S. J. Vac. Sci. Technol., A* **2019**, *194*, 156.
- (19) Li, X.; Rafie, A.; Kalra, V.; Lau, K. K. *S. Langmuir* **2020**, *36*, 13079.
- (20) Liu, W.; Li, X.; Ye, Y.; Wang, H.; Su, P.; Yang, W.; Yang, Y. *J. Energy Chem.* **2022**, *66*, 30.
- (21) Zhou, Y.; Wang, X.; Acauan, L.; Kafon-Cohen, E.; Ni, X.; Stein, Y.; Gleason, K. K.; Wardle, B. L. *Adv. Mater.* **2019**, *31*, 1901916.
- (22) Zhang, L.; Viola, W.; Andrew, T. L. *ACS Appl. Mater. Interfaces* **2018**, *10*, 36834.
- (23) Xu, G. L.; Liu, Q.; Lau, K. K. S.; Liu, Y.; Liu, X.; Gao, H.; Zhou, X.; Zhuang, M.; Ren, Y.; Li, J.; Shao, M.; Ouyang, M.; Pan, F.; Chen, Z.; Amine, K.; Chen, G. *Nat. Energy* **2019**, *4*, 484.
- (24) Su, L.; Smith, P. M.; Anand, P.; Reeja-Jayan, B. *ACS Appl. Mater. Interfaces* **2018**, *10*, 27063.
- (25) Zhang, Y.; Kim, C. S.; Song, H. W.; Chang, S. -J.; Kim, H.; Park, J.; Hu, S.; Zhao, K.; Lee, S. *Energy Storage Mater.* **2022**, *48*, 1.
- (26) Heydari Gharahcheshmeh, M.; Wan, C. T. C.; Ashraf Gandomi, Y.; Greco, K. V.; Forner-Cuenca, A.; Chiang, Y. M.; Brushett, F. R.; Gleason, K. K. *Adv. Mater. Interfaces* **2020**, *7*, 2000855.
- (27) Clevenger, M.; Kim, H.; Song, H. W.; No, K.; Lee, S. *Sci. Adv.* **2021**, *7*, eabj8958.
- (28) Muralter, F.; Coclite, A. M.; Lau, K. K. S. *Adv. Electron. Mater.* **2021**, *7*, 2000871.
- (29) Kim, J. J.; Fan, R.; Allison, L. K.; Andrew, T. *Sci. Adv.* **2020**, *6*, eabc3296.